# Structure and Mechanism of Action of Riboflavin-Binding Protein: Small-Angle X-Ray Scattering, Sedimentation, and Circular Dichroism Studies on the Holo- and Apoproteins[1]

THOMAS F. KUMOSINSKI, HELMUT PESSEN, AND HAROLD M. FARRELL, JR.

Riboflavin-binding protein, a transport protein occurring in egg whites, binds riboflavin tightly at pH values above 4.5 but releases it readily at pH values below 4.0. Structural aspects of this biologically important binding were studied by several methods. Analysis of sedimentation equilibrium data gave an average molecular weight of 32,500 ± 1000 for all forms of the protein and showed the absence of changes in quaternary structure when riboflavin was bound at neutral pH or released at pH 3.7. Sedimentation velocity showed no change in tertiary structure on binding at pH 7.0 but revealed a significant change in sedimentation constant at pH 3.7. While circular dichroism showed no appreciable change in secondary structure, it gave evidence of a marked change in the aromatic region at the lower pH. Small-angle X-ray scattering, going from the holoprotein at neutral pH to the apoprotein at low pH, showed a small but significant increase in radius of gyration (19.8 ± 0.2 vs 20.6 ± 0.1 Å) with slightly decreased anisotropy and with substantial increases in molecular volume (55,600 ± 530 vs 66,500 ± 240 $Å^3$), surface (11,840 ± 120 vs 13,470 ± 140 Å), and hydration (0.27 ± 0.01 vs 0.38 ± 0.01 g $H_2O$/g dry protein). Hydration values were obtained from small-angle X-ray scattering in two different ways for comparison with those calculated from sedimentation coefficients by way of frictional coefficients (derived from two different dimensionless ratios based independently on the structural small-angle X-ray scattering data). For either form of the protein, the surface calculated from an ellipsoidal model could account for only about 62% of the surface found experimentally. The excess surface was ascribed to topographic features of the molecule. Relative changes in this new parameter, together with the circular dichroism data and the known association of riboflavin binding with aromatic residues, suggested the opening of an aromatic-rich cleft concomitant with the release of riboflavin as a consequence of lowered pH.

[1] This paper is dedicated to Professor Dr. Otto Kratky on the occasion of his 80th birthday in recognition of his preeminent role in the development and application of the small-angle X-ray scattering method and in appreciation of his inspiration to several generations of workers in the field. Preliminary reports of this work were presented at the 160th, 162nd, and 180th National Meetings of the American Chemical Society, in 1970, 1971, and 1980.

Riboflavin-binding protein (RBP)[2] occurs in the yolks and whites of all avian eggs tested so far (1). The absence of this protein from the blood and eggs of a mutant strain of chickens leads to the death

[2] Abbreviations used: RBP, riboflavin-binding protein; SAXS, small-angle X-ray scattering; SDS, sodium dodecyl sulfate.

of the developing embryo by reason of a gross riboflavin deficiency (2, 3). Thus, RBP is shown to be responsible for the transport of riboflavin through the blood stream of the laying hen and into the eggs, where the vitamin is essential for embryonic growth and development (4, 5). Studies of the reversible binding of riboflavin to RBP have yielded values for the association constant of $10^9$ to $10^{10}$ $M^{-1}$ (6, 7). This strong binding serves the function of transport well, but it is not known how it is overcome so that the vitamin is released to the embryo. However, the pH profile for binding of riboflavin to the protein shows that below pH 4.0 the binding drops off rapidly, with an apparent p$K$ at 3.8 (8, 9). The release of riboflavin at acid pH could be due to protonation of specific residues or to more generalized phenomena relating to changes in the structure of the protein.

Neither the amino-acid sequence nor the X-ray crystallographic structure of RBP is known. In the absence of such basic structural information, this study takes an alternative approach in which a variety of techniques are employed in a joint examination of some aspects of the secondary and tertiary structure of the protein pertinent to the mechanism of binding. A number of parameters relating to the protein both above and below the p$K$ of binding are obtained from small-angle X-ray scattering (SAXS). These, together with data from sedimentation velocity and equilibrium, circular dichroism, and gel electrophoresis, are used for correlating observed structural changes with the binding and release of riboflavin by RBP.

## MATERIALS AND METHODS

*Materials and sample preparation.* RBP was prepared by the method of Farrell *et al.* (8) and analyzed for purity electrophoretically on SDS gels by the method of Laemmli (10) with the use of 10% acrylamide. This method was used also to estimate the molecular weight of RBP, with bovine serum albumin, ovalbumin, $\beta$-lactoglobulin, and $\alpha$-lactalbumin as standards at 68,000, 45,000, 19,000, and 15,000, respectively.

Sample solutions were prepared by dissolving the protein in 4 to 6 ml of the appropriate solvent, adjusting the pH to the desired value, and dialyzing against three 1-liter changes of solvent. Required dilutions were made with the final dialyzate. Protein concentrations were determined by the method of Lowry *et al.* (11) or by the use of the molar absorption coefficient of $4.9 \times 10^4$ $M^{-1}$ $cm^{-1}$ (12) for the apoprotein at 282 nm. SAXS measurements were carried out at concentrations from about 13 to 78 g/liter, at pH 3.7 in 0.005 M phosphate buffer containing 0.1 M NaCl for the apoprotein and at pH 7.0 in 0.005 M phosphate containing 0.1 M NaCl for both apoprotein and holoprotein. The same buffers were used for spectral measurements, but increased phosphate (0.03 M) was used for the ultracentrifuge studies. All buffer chemicals were reagent grade. Samples for absorption and circular dichroism spectra as well as for analytic ultracentrifugation were filtered through 0.22-$\mu$m Millipore[3] filters.

All samples were kept in the dark at 0 to 5°C until immediately prior to use in order to preclude the possibility of photooxidation of riboflavin (13). Oxidation products of riboflavin were monitored fluorometrically as described by Koziol (14). Exposure of samples to irradiation (in the uv and visible regions) generated by either the Cary-14 or the JASCO spectropolarimeter resulted in no increase in $CHCl_3$-extractable products over those obtained from solutions which had never been exposed to light. Riboflavin purchased commercially had between 0.4 and 0.7% of these compounds present.

*SAXS measurements and data evaluation.* The apparatus employed was an absolute-scale small-angle X-ray scattering instrument designed and constructed at this laboratory. It is a directly referenced, symmetrically scanning, vertical-axis instrument with sealed-window proportional detection, used in the continuous-scan mode with appropriately long time constants. The $CuK_{\alpha 1}$ radiation from a fine-focus tube operated at 40 kV and 25 mA was selected by the curved quartz-crystal primary-beam monochromator. Other apparatus details as well as data and results obtained with this instrument have been presented and critically discussed (15–17). Measurement procedures in this study were those described in detail previously (16, 17).

The working equations and the notations used are essentially those of Luzzati *et al.* (18, 19), with some modifications. They apply to globular particles in the case of so-called "infinite slit" collimation (i.e., very high slit height-to-width ratio), conditions satisfied by the instrument and the systems under examination. The equation (18) relating the scattered intensity $j_n(s)$ (scattered intensity of sample, normalized with respect to the intensity of the incident beam

[3] Reference to brand or firm name does not constitute endorsement by the U. S. Department of Agriculture over others of a similar nature not mentioned.

and corrected for scattering of blank) to the scattering angle $2\theta$ is:

$$j_n(s) = j_n(0) \exp[-(4/3)\pi^2 R_a^2 s^2] + \phi(s), \quad [1]$$

where $s = (2 \sin \theta)/\lambda$; $\lambda$ is the wavelength of the radiation used (1.540 Å); $j_n(0)$ is the normalized intensity extrapolated to zero angle; $R_a$ is the apparent radius of gyration obtained by slit collimation at a finite concentration of solute (20); and $\phi(s)$ is a function expressing the residual between the gaussian part of Eq. [1] and the scattering actually observed. For small values of $s$ (i.e., $s < 2.5 \times 10^{-2}$ Å$^{-1}$, or $2\theta < 2°$), $\phi(s)$ is always negligible compared with the first term, which represents the Guinier approximation (21). $R_a$ can therefore be obtained from the gaussian fit to $j_n(s)$ vs $s^2$ for the region of very small angles. Since, however, the theoretical point-source scattering function $i_n(s)$ was needed later in any event, it was constructed from the smeared infinite-slit data $j_n(s)$ by deconvolution (18), and the concentration-dependent point-source radius of gyration $R_i$ was, in fact, obtained in place of $R_a$ in an analogous manner.

After evaluating $i_n(0)$ by extrapolation of $i_n(s)$ to zero angle, it was possible to calculate

$$m_{app} = i_n(0)(1 - \rho_1\psi_2)^{-2} c_e^{-1}, \quad [2]$$

$$m = m_{app} + 2Bm^2 c_e, \quad [2a]$$

and

$$M = mN_A/q. \quad [2b]$$

Here $m_{app}$ is the apparent molecular mass, expressed as electrons per molecule, at concentration $c_e$; $c_e$ is the concentration in electrons of solute per electron of solution; $m$ is the molecular mass obtained by extrapolation to zero concentration of a plot of $m_{app}$ vs $c_e$; $\rho_1$ is the electron density of the solvent, calculated as 0.355 electrons/Å$^3$; $\psi_2$ is the electron partial specific volume of the solute, $\psi_2 = 10^{24}\ \bar{v}/q = 2.376$ Å$^3$/electron, where $\bar{v}$ is the partial specific volume of the protein, 0.720 ml/g, and $q$ is the number of electrons per gram of particle, $0.303 \times 10^{24}$, both calculated from the amino acid composition (8). (A value of $\bar{v}$ = 0.720 ml/g was found earlier also by Phillips (22) from sedimentation equilibrium data for this protein measured in $H_2O$ and $D_2O$.) $2B$ is the second virial coefficient; $M$ is the weight-average molecular weight; and $N_A$ is Avogadro's number.

Introduction of a corrected normalized scattering intensity $j_n^*(s)$ defined by

$$j_n^*(s) = j_n(s) - \delta^*, \quad [3]$$

where $\delta^*$ is a correction term reflecting short-range electron-density fluctuations due to the internal structure of the particle, leads to the equation,

$$s^3 j_n^*(s) = s^3 j_n(s) - \delta^* s^3, \quad [3a]$$

illustrated by the Soulé-Porod plots (23, 24) of $s^3 j_n(s)$ vs. $s^3$ (cf. Fig. 1B). The straight line fitted to such a plot at intermediate and higher values of $s$, where the gradually diminishing oscillations of the curve permit a fairly reliable fit of a straight line as a mean, provides an asymptotic approximation represented by

$$\lim_{s\to\infty} s^3 j_n(s) = \lim_{s\to\infty} s^3 j_n^*(s) + \delta^* s^3, \quad [3b]$$

which allows the evaluation of the constants $\delta^*$ and $\lim_{s\to\infty} s^3 j_n^*(s)$ (both needed for subsequent expressions derived by Luzzati) from the slope and intercept of the asymptote, respectively. (To be strictly consistent, $j_n^*(s)$ should have been used in place of $j_n(s)$ in Eq. [1], but the value of $R_a$ is not actually affected by the correction of $\delta^*$ (18), in contrast to the equations that follow.)

With the use of these constants, further parameters were calculated (18):

$$V = i_n(0) \Big/ \int_0^\infty 2\pi s j_n^*(s) ds; \quad [4]$$

$$S/V \simeq \frac{16\pi^2 \lim_{s\to\infty} s^3 j_n^*(s)}{\int_0^\infty 2\pi j_n^*(s) ds} \left[1 - \frac{c_e\rho_2(1 - \rho_1\psi_2)}{\rho_2 - \rho_1}\right]; \quad [5]$$

$$\Delta\rho = \rho_2 - \rho_1 \simeq \frac{\int_0^\infty 2\pi s j_n^*(s) ds}{c_e(1 - \rho_1\psi_2)} + c_e\rho_1(1 - \rho_1\psi_2); \quad [6]$$

$$H = \frac{\rho_1(1 - \rho_2\psi_2)}{\Delta\rho}. \quad [7]$$

Here $V$ is the hydrated volume; $S$ is the external surface area of the particle; $\rho_2$ is the mean electron density of the hydrated particle, in electrons per cubic angstrom; S/V is the surface-to-volume ratio; and $H$ is the degree of hydration in electrons of bound $H_2O$ per electron of dry particle, from which the conventional degree of hydration, expressed as the number of grams of water of hydration per gram of dry protein, can be obtained by a simple conversion. Tabulated parameters (such as the point-source radius of gyration $R_G$, derived from the concentration-dependent point-source radius of gyration $R_i$) were obtained by extrapolation to zero concentration.

*Sedimentation analysis.* Sedimentation equilibrium studies by the Yphantis meniscus depletion method (25) were performed on a Beckman Model E analytical ultracentrifuge equipped with electronic speed control and photometric scanner. The scanner was interfaced with a Modular Computer Systems Model III computer equipped with a real-time analog-to-digital voltmeter set to take readings at 40-ms intervals. For a medium-speed scan of an equilibrium boundary with a 0.2-cm column height, at least 60 data points were obtained by this procedure. For each solution and its corresponding solvent blank, a minimum of 25 separate scans were averaged to maxi-

mize the precision to a theoretical value of ±0.002 absorbance units. The averaging routine was performed by specially developed computer programs to be described in a future publication.

Weight-average molecular weights were obtained by use of the exponential function (26) derived by integration of the general expression,

$$\int_{c_0}^{c} dc/c = \int_{r_a}^{r} \sigma_w r dr, \quad [8]$$

which results in

$$c = c_0 \exp[\sigma_w(r^2 - r_a^2)/2], \quad [9]$$

where $\sigma_w = M_w\omega^2(1 - \bar{v}\rho)/RT$, $M_w$ is the weight-average molecular weight, $\omega$ is the rotor speed in radians per second, $\bar{v}$ is the partial specific volume, $\rho$ is the density of solvent, $R$ is the ideal gas constant, $T$ is the temperature in degrees Kelvin, $c$ is the concentration at a position $r$ from the center of rotation in centimeters, and $c_0$ is the concentration at the meniscus, positioned at a distance $r_a$ from the center of rotation. This exponential function was fitted to the data points by means of a computer program developed at this laboratory which uses a nonlinear iterative Gauss-Newton regression analysis. Molecular weights thus determined are precise, and the fit reflects the homogeneity of the sample.

Sedimentation velocity experiments with the same data collection system resulted in a minimum of 200 points per boundary. Each boundary was analyzed by a fit of an integral of a gaussian, again by the Gauss-Newton procedure. For each experiment, a minimum of 15 scans were used to obtain a linear regression of the log of the distance of the boundary from the center of rotation as a function of time. From the regression coefficient, $s_{20,w}$ was calculated with a precision of ±0.1%. Such an analysis is equivalent to a second-moment calculation for schlieren data, and any existing heterogeneity of the sample can be verified easily by the nonlinearity of the log of the position vs. time plot (27). An additional benefit of the scanner over the schlieren or fringe optical system is that it provides, by virtue of the high sensitivity of absorbance measurements at 280 nm, the means of working at very dilute (<1 mg/ml) protein concentrations. The nonidealities arising from hydrodynamic drag and virial effects are thus bypassed and, since the protein studied is monomeric, it was not necessary to perform concentration dependence studies of $s_{20,w}$. Under these conditions, sedimentation equilibrium results also would have negligible contributions from virial coefficients (28).

*Circular dichroism.* Spectra were recorded at ambient temperature on a JASCO Model J-41C spectropolarimeter. Measurements were carried out on diluted protein solutions in 1.0-cm pathlength cells for visible and near uv and in 0.05-cm pathlength cells for the far uv. In the far uv region (200 to 240 nm), the results, reported as $\Theta_{mrw}$, were calculated from the mean amino acid residue weight by the method of Chen *et al.* (29), with a mean residue weight of 118. In the visible and near uv region, the results, $\Theta_m$, are expressed in terms of the molar ellipticity of the protein in degrees-square centimeter-deciliter mole$^{-1}$.

## RESULTS

### *Small-Angle X-ray Scattering*

Typical Guinier plots, constructed according to Eq. [1], are shown in Fig. 1A; from the slopes of corresponding plots of slit-corrected data (not shown), $R_i$ values were obtained in analogy to the $R_a$ in this equation. Similarly, several Soulé-Porod plots, constructed from slit-source data according to Eq. [3a], are shown in Fig. 1B. From the values of the constants $\lim_{s\to\infty} s^3 j_n^*(s)$, obtained as ordinate intercepts of the straight lines fitted by linear regression to the portions of these plots starting from the first maximum and minimum, the parameters given by Eqs. [4] to [7] were calculated.

After transformation of slit-source data to point-source data (16), $M$ was obtained by Eq. [2], and the remaining parameters (Eqs. [1] and [4] to [7]) were calculated for each concentration at which observations had been made. The concentration dependences of the six parameters $R_G$, $V$, $S/V$, $M$, $\Delta\rho$, and $H$ are shown in Fig. 2 with five concentrations of the holoprotein at pH 7.0 and four concentrations of the apoprotein at pH 3.7. Except for $V$ and $M$, dependence on concentration is absent or negligible. For both $V$ and $M$, however, all slopes are negative; this is in accord with the virial coefficients implicit in Eqs. [2] and [4]. The values resulting from extrapolation for the two forms of the protein are listed in Table I. Also listed in the table are values for the axial ratios calculated for model spheroids of half-axes $a$ and $b$ (where $a > b$). These were calculated in two ways (designated by subscripts 1 and 2), according to whether the expression $3V/(4\pi R_G^3)$ or $R_G(S/V)$ was utilized to evaluate $a/b$ (18). The significance of the difference between these quantities is discussed further on.

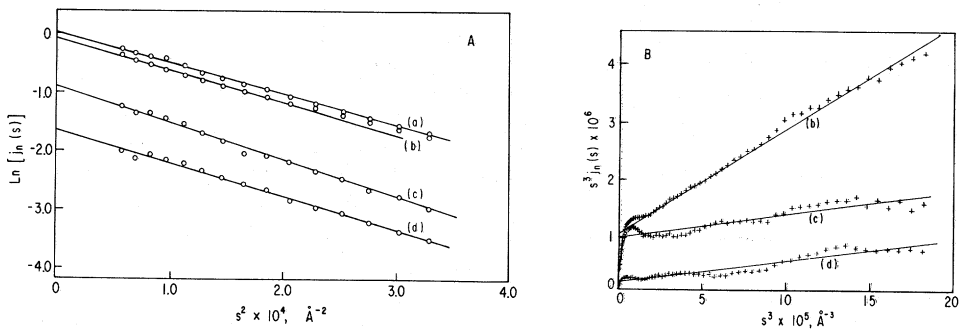


FIG. 1. Typical scattering functions from slit-smeared data (for apoRBP at pH 3.7 in 0.005 M phosphate and 0.1 M NaCl) at several concentrations: (a) 70.9; (b) 62.9; (c) 21.0; and (d) 12.6 g/liter. (A) Semilogarithmic plot of normalized slit-source scattering intensity vs square of scattering angle (Guinier plot). (B) Plot of $s^3 j_n(s)$ vs $s^3$ (Soulé-Porod plot).

*Sedimentation*

Sedimentation equilibrium data were fitted by an exponential function as described in the experimental section, for both the holo and apo forms of the protein at pH 7.0 and for the apo form at pH 3.7. An exponential function for a simple monomer system shows a good fit to representative time-averaged data for the apoprotein at pH 7.0 (Fig. 3), indicating no heterogeneity by either self-association or high molecular-weight impurities. Equilibrium data for both the apoprotein at pH 3.7 and the holoprotein at pH 7.0 gave equally good agreement. Molecular weights for all three samples were within ±3%, resulting in an average of 32,500. For this reason, the possibility of aggregation occurring as a function of pH or the binding of riboflavin can be ruled out.

Polyacrylamide gel electrophoresis (hereafter referred to simply as electrophoresis) in the presence of sodium dodecyl sulfate showed the protein to be homogeneous and to be composed of a single polypeptide chain with a reduced molecular weight of 34,000 ± 2000. This is in general agreement with the monomer molecular weight obtained by sedimentation equilibrium and SAXS.

Since no heterogeneity was detectable by sedimentation equilibrium or electrophoresis for any samples, sedimentation velocity experiments were performed under the same conditions as the equilibrium

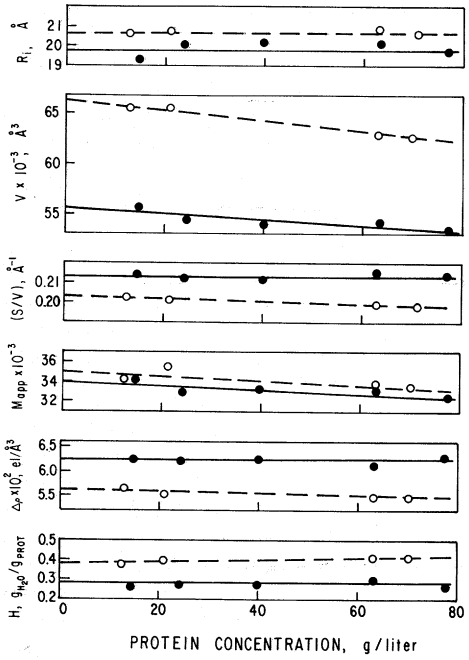


FIG. 2. Concentration dependence of six molecular parameters (radius of gyration, hydrated volume, surface-to-volume ratio, molecular weight, electron density difference, degree of hydration) for RBP holoprotein (●) and apoprotein (○). Experimental conditions as described under Materials and Methods. Concentration dependence of $V$ and $M$ is readily apparent for both forms of the protein. Slopes of $S/V$, $\Delta\rho$, and $H$ for apoprotein are very slight and of doubtful physical significance, but because inspection suggests such slopes, the intercepts at zero concentration, rather than the means, were used in these cases also as the values of the respective parameters listed in Table I.

TABLE I

SAXS PARAMETERS OF RBP[a]

| Parameter[b] | Form of protein: Holoprotein (pH 7.0) | Form of protein: Apoprotein (pH 3.7) |
|---|---|---|
| $R_G$(Å) | 19.8 ± 0.2 | 20.6 ± 0.1 |
| $V$(Å$^3$) | 55,600 ± 530 | 66,500 ± 240 |
| $S/V$(Å$^{-1}$) | 0.213 ± 0.001 | 0.203 ± 0.001 |
| $M$ | 33,800 ± 400 | 35,000 ± 800 |
| $\Delta\rho$ (electrons/Å$^3$) | 0.0625 ± 0.0005 | 0.0563 ± 0.0004 |
| $H$ (g $H_2O$/g dry protein) | 0.27 ± 0.01 | 0.38 ± 0.01 |
| $(a/b)_1$ (from $3V/(4\pi R_G^3)$) | 1.77 ± 0.05 | 1.63 ± 0.03 |
| $(a/b)_2$ (from $R_G(S/V)$) | 3.62 ± 0.04 | 3.57 ± 0.05 |

[a] Error terms represent the standard error of the parameter. For $R_G$, which was concentration-independent as were $S/V$, $\Delta\rho$, and $H$ in the case of the holoprotein, this is the standard deviation of the mean; for $V$, $M$, and in the case of the apoprotein also $S/V$, $\Delta\rho$, and $H$, it is the standard error of the intercept (see also legend to Fig. 2); for the derived parameters $(a/b)_1$ and $(a/b)_2$, it is the value calculated by error propagation from the primary parameters.

[b] Definitions and procedures for obtaining these parameters are as given under Materials and Methods.

experiments. A representative individual scan of a velocity experiment (Fig 4) shows a good fit of an integral of a gaussian to 200 data points, further indicating homogeneity of the sample. Sedimentation coefficients derived from such an analysis with a precision of ±0.01S are given in Table II for all forms of RBP. Holo- and apoRBP at pH 7.0 have $s_{20,w}$ values which are essentially the same, indicating the lack of influence of riboflavin binding on the tertiary structure of the protein. ApoRBP at pH 3.7, on the other hand, gives an $s_{20,w}$ smaller than at pH 7.0, which could mean large changes in hydration, tertiary structure, or both.

*Circular Dichroism*

Circular dichroism experiments were performed on apoRBP at both pH values to observe the extent of secondary structural changes. Figure 5A shows the far uv CD spectra for both forms of apoRBP.The protein at pH 3.7 shows slight changes in negative ellipticity between 210 and 230 nm as well as a small increase at 205 nm. These changes may be indicative of less ordered structure at pH 3.7. Examination of the near uv CD spectra (Fig. 5B) shows significant decreases in negative ellipticity in the chromophoric region, and this too supports the suggestion of increased disorder in the protein below pH 4.0. The CD spectra for holoRBP are given at pH 7.0 for the near uv and visible region (Fig. 6). These spectra along with those of apoRBP at pH 7.0 are in excellent agreement with previously published data (7); however, no spectra below pH 4.0 are available for comparison.

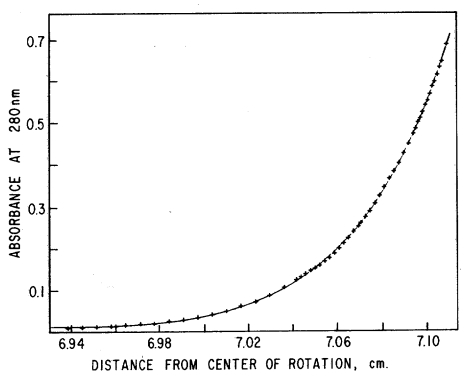


FIG. 3. Sedimentation equilibrium of holoRBP, pH 7.0, in 0.1 M NaCl, 0.03 M $NaHPO_4$, 25°C, in 1.2-cm, cell at 8000 rpm; (+) time-averaged data; (——) best fit for a simple monomer.

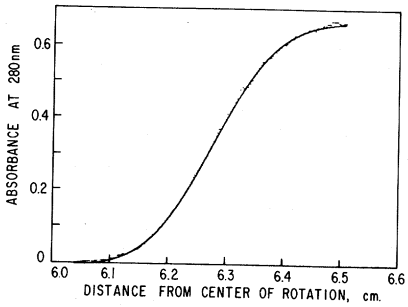


FIG. 4. Sedimentation velocity of apoRBP, pH 7.0, in 0.1 M NaCl, 0.03 M $NaHPO_4$, 25°C, in 1.2-cm cell at 52,000 rpm; time, 80 min; points are experimental data; solid line represents best fit for an integral of a gaussian.

TABLE II

SEDIMENTATION VELOCITY RESULTS

| | pH | $s_{20,w}$,S | $(f/f_0)_T$[a] | $(f/f_0)_1$[b] | $(f/f_0)_2$[c] |
|---|---|---|---|---|---|
| HoloRBP | 7.0 | 2.92 | 1.30 | 1.03 | 1.16 |
| ApoRBP | 7.0 | 2.91 | 1.30 | — | — |
| ApoRBP | 3.7 | 2.70 | 1.40 | 1.02 | 1.15 |

[a] $(f/f_0)_T = 1.20 \times 10^{-15}\ M^{2/3}\ (1 - \bar{v}\rho_0)/(s_{20,w}\bar{v}^{1/3})$, where $M$ = 32,500, $\bar{v}$ = 0.720, and $\rho_0$ = density of $H_2O$ at 20°C. See Ref. (35).

[b] From $(a/b)_1$. See Table I and Ref. (18), and Perrin's equation, Ref. (36).

[c] From $(a/b)_2$. See Table I and Ref. (18), and Perrin's equation, Ref. (36).

## DISCUSSION

Comparison between the SAXS parameters in Table I for the two forms of the protein at pH 7.0 and pH 3.7 shows that, in going from the holo to the apo form, the radius of gyration increases from 19.8 to 20.6 Å. The difference of 0.82 (with a standard deviation of the difference of the means of 0.19 Å) is relatively small but statistically significant. It is of the same order of magnitude, and in the same direction, as comparable changes in radius of gyration found by other workers from SAXS in cases of protein binding of ligands of roughly similar size. For yeast hexokinase, Steitz and co-workers (30, 31) found that on binding glucose there was a reduction in radius of gyration of 0.95 ± 0.24 Å; on binding glucose 6-phosphate the reduction was 1.25 ± 0.28 Å. On binding 3-phosophoglycerate to phosphoglycerate kinase there was a 1.09 ± 0.34 Å reduction (32). Quiocho *et al.* (33), studying similar changes in a number of sugar-binding proteins, determined a decrease of 0.94 ± 0.33 Å in radius of gyration upon binding of arabinose to L-arabinose-binding protein. In these instances, the X-ray crystallographic structures were known, and radii of gyration computed from them were in close agreement with those found from SAXS. The X-ray data further showed a clear conformational difference between apo and holo forms of the protein and indicated that the mechanism of binding depended on an allosterically induced closure of a cleft in the molecule. Except for the radius of gyration, no other structural SAXS parameters were used in the study of these systems; in fact, in no case

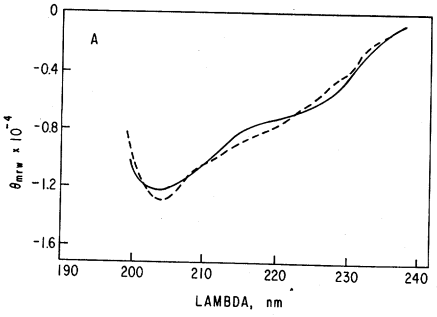


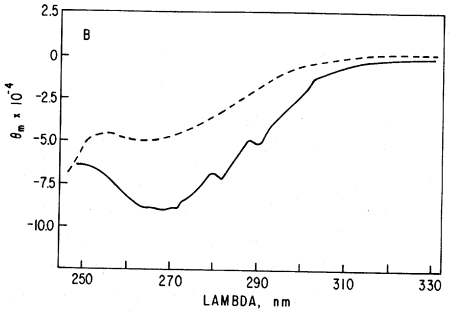


FIG. 5A. CD spectra of apoRBP in the far uv region at pH 3.7 (- - -) and pH 7.0 (——). Each curve represents the average of 16 accumulated spectra.

FIG. 5B. CD spectra of apoRBP in the near uv region at pH 3.7 (- - -) and 7.0 (——). Each curve represents the average of four accumulated spectra.

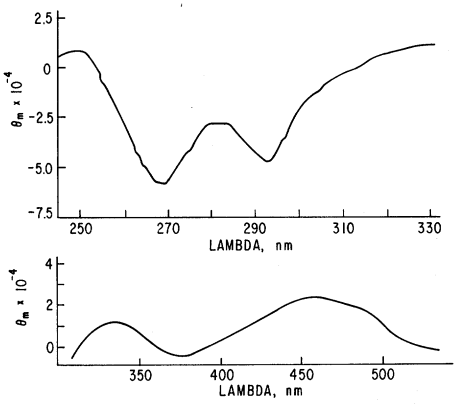


FIG. 6. CD spectra obtained for holoRBP at pH 7.0. The near uv (upper curve) and visible (lower curve) data are the average of four and two accumulated spectra, respectively.

were any SAXS parameters, such as $V$, $S/V$, $a/b$, or $H$, reported.

The SAXS molecular weights are listed for information only, since more accurate molecular weights can be determined by sedimentaion equilibriuim, as discussed later. The volume and surface-to-volume changes, on the other hand, are significant and warrant discussion.

The marked increase in volume accompanying release of the riboflavin at low pH must be indicative of swelling, due to increased hydration, structural changes, or both. The increase in $H$ from 0.27 to 0.38 g $H_2O$/g dry protein shows that hydration certainly is a factor; it corresponds to a presumptive increase from about 500 to 700 molecules of water per protein molecule. But even allowing a volume of 30Å$^3$ per molecule of water (estimated from the specific volume of bulk water), the difference of about 200 molecules could account for at most about 7000 Å$^3$ of the 10,900-Å$^3$ increase in hydrated volume seen from Table I. A considerable amount of structural swelling must, therefore, occur, perhaps owing to the reversal of net charge, since the protein at pH 3.7 is below its isoelectric point, and also because of increased segmental motion of side chain groups. We return to this matter on discussing the CD findings below.

Inspection of the relative changes in several of the parameters (+4% for $R_G$, +20% for $V$, −5% for $S/V$) discloses that they are roughly consistent with one another from simple dimensional considerations, although the change in $R_G$ is slightly less than would be expected from the corresponding changes in $V$ and $S/V$. This is a hint of some decrease in anisotropy. A combined consideration of the parameters leads to some further information. Since the expression $3V/(4\pi R_G^3)$ is dimensionless, it must be characteristic of a family of spheroids of equal anisotrophy and must be a function of the axial ratio $a/b$ only (18). Conversely, $a/b$ can be calculated from the dimensionless ratio (by straightforward numerical methods, if not in closed form). The values listed in Table I as $(a/b)_1$ show that there is indeed a small but significant decrease from 1.77 to 1.63; i.e., the molecule at pH 3.7 has become somewhat more rounded as well as bulkier. If the molecule is regarded as a prolate ellipsoid of revolution one may, from the values of $a/b$ and $V$, obtain the values of the respective half-axes ($a = 34.6 \pm 0.6$, $b = 19.6 \pm 0.2$ Å, for the holoprotein; $a = 34.8 \pm 0.5$, $b = 21.4 \pm 0.2$ Å for the apoprotein). The differences between the parameters of holo- and apoRBP in every one of the preceding instances, as well as in nearly all of those to follow, are statistically significant (by $t$ test, $P < 0.01$, in all cases except for $\Delta\rho$ and $(a/b)_2$, where $P \simeq 0.1$, and $a$, where $P > 0.2$). The difference in $a$ is thus not significant at any reasonable probability level. It may, therefore, be concluded that both the decrease in anisotropy and the increase in volume are due mainly to an enlargement of the minor axis.

The axial ratio $(a/b)_2$ is obtained from the second dimensionless ratio used by Luzzati *et al.* (18), $R_G(S/V)$. This, in contrast to the first, includes a parameter that is a measure of surface. The resulting value (holoRBP, 3.62; apoRBP, 3.57) clearly does not represent a "real" ellipsoid but some equivalent ellipsoid of identical volume. This second model attempts to compensate in terms of the smooth surface of a hypothetical, elongated body for the textured surface of the more compact actual body, which would not be amenable to

characterization by two simple parameters ($a$ and $b$). These parameters, since they are based on three independent equations (one for each of the experimental quantities $R_G$, $S$, and $V$), are algebraically overdetermined and will not yield a calculated value for $R_G$ identical to the experimental one. Nonetheless, since it does take into account surface features, this may be a useful alternative model to employ for comparisons with the surface-sensitive data obtained from hydrodynamic phenomena.

To examine the data relating to surface area more closely, it will be convenient to distinguish between several separate contributions to the total surface. First, there is the surface of the basic model, i.e., the ellipsoid of revolution having the volume and radius of gyration found by SAXS independently of any model assumptions. Its surface area, as a first approximation to that of the molecule, may be designated as $S_M$, the model surface. Second, it is recognized that the assumption of an ellipsoid of revolution is arbitrary and is made only as a point of departure because of its mathematical convenience. The real model is certain to vary from this idealization and to be less readily characterized. A closer approximation might be some other shape, such as an ellipsoid of three different axes, a cylinder or conical frustum with rounded edges, or a kidney. Without attempting to go into details of such geometries, we may assume that for any such body with identical volume and radius of gyration the corresponding surface area will be somewhat larger than $S_M$. To take the difference into account, we consider it as an excess surface, $S_B$, the additional contribution to surface due to deviation in overall body shape from the spheroidal model. Third, it is obvious that the surface of a molecule which consists of coiled, folded, and unordered chains, as does a protein, cannot be smooth. Superimposed on the body shape will be such textural features as wrinkles, small protuberances, clefts, or localized grooves. These will make a substantial contribution to surface which we designate as $S_X$, the additional contribution to surface due to texture. When convenient, $S_B$ and $S_X$ might be lumped together as $S_T$, the excess topographical surface. If we assign all conceivable contributions to total surface to one of the three categories, $S_M$, $S_B$, or $S_X$, then $S_M + S_B + S_X$ must equal $S_{tot}$, the total surface area.

As a measure of $S_{tot}$ we take the surface $S$ found from experiment. Using the respective values for $V$ and $S/V$ from Table I, we have $S_{tot}$ equal to 11,840 ± 120 Å$^2$ for holoRBP and 13,470 ± 140 Å$^2$ for apoRBP. For $S_M$, using the appropriate geometric expression for elliptical surface in terms of $a$ and $b$, we calculate 7420 ± 30 and 8250 ± 30 Å$^2$, respectively. It is noteworthy that the ratio $S_M/S_{tot}$ is 0.63 ± 0.01 and 0.61 ± 0.01, respectively. It follows that $S_T/S_{tot}$, the remaining fraction of about 0.38, also is the same, or nearly so, for both forms of the protein; i.e., the increased $S_{tot}$ remains divided in nearly the same proportions between $S_M$ and $S_T$. Even without specific knowledge of $S_B$ (obtainable, for example, from a more detailed shape analysis by use of distance-distribution functions), there is some pertinent information available because the shape of a scattering particle gives rise to very characteristic fluctuations in the various scattering curves, as discussed, e.g., by Kratky (34) and as seen in the Soulé-Porod plots of Fig. 1B. Shapes and positions of the minima and maxima in this figure did not change between apoprotein and holoprotein (the latter not shown here), and similar minima and maxima in the tails of the primary scattering curves (e.g., $j_n$ ($s$) vs $s$), where they show up even more sharply, remained equally undisplaced. Whatever $S_B$ might be, it thus cannot differ by much between the two forms of RBP in the absence of a change in body type or any major change in shape within the same body type. From a consideration of the behavior of $S_{tot}$, $S_N/S_{tot}$, and $S_B$, it may be concluded that at low pH not only does $S_X$ increase in absolute terms, but as a fraction of total surface it must also increase to some extent depending on $S_B$. That is, the new textural surface must be in proportion to the new total surface or more. A structural change to fit this geometry would be pro-

TABLE III

DERIVED HYDRATION RESULTS[a]

| | pH | $h_1$[b] | $h_2$[c] | $H'$[d] | $H$[e] |
|---|---|---|---|---|---|
| HoloRBP | 7.0 | 0.73 | 0.29 | 0.31 | 0.27 |
| ApoRBP | 3.7 | 1.14 | 0.57 | 0.51 | 0.38 |

[a] All $h$ and $H$ values in g $H_2O$/g dry protein.

[b] $h_1 = \{[(f/f_0)_T/(f/f_0)_1]^3 - 1\}\bar{v}\rho_0$. See Refs. (27, 40).

[c] $h_2 = \{[(f/f_0)_T/(f/f_0)_2]^3 - 1\}\bar{v}\rho_0$. See Refs. (27, 40).

[d] $H' = [(VN_A/10^{24}M) - \bar{v}]\rho_0$, where $V$ is the volume of the molecule from SAXS (Table I), $M$ is the molecular weight, 32,500, $N_A$ is Avogadro's number, and $\rho_0$ is the density of water in g/ml. See Refs. (27, 34, 40).

[e] From SAXS (Table I).

vided by a cleft which opens to supply this increased textured surface, as well as the sites of additional hydration and, by the concomitant swelling, the increased volume and radius of gyration measured. This increase in radius of gyration, it may be noted, is nearly the same as corresponding increases documented in other cases of cleft mechanisms, where clefts accomodate ligands of the same order of size (30–33).

Time-averaged sedimentaion equilibrium data showed no heterogeneity in samples of RBP under any of the environmental conditions studied (Fig. 3) and gave an average molecular weight of 32,500 ± 1000. Molecular weights derived from SAXS (Table I) and electrophoresis were slightly higher. However, since equilibrium data are more accurate than SAXS and electrophoresis results and it is well established that molecular weights derived from sedimentation equilibrium at low concentrations can be considered to be the anhydrous value (27), the value of 32,500 was chosen for all hydrodynamic calculations.

Sedimentation velocity results (Table II) clearly show changes in $s_{20,w}$ under acid conditions but indicate no change as a result of the binding of riboflavin at pH 7.0, in contrast to other systems such as hexokinase (30, 31) and L-arabinose-binding protein (33). In these systems, changes in tertiary structure result from the binding of ligand at neutral pH. Hydrodynamic frictional ratios $(f/f_o)_T$, derived from $s_{20,w}$ and the relationship in Table II (35), which were the same for the holo and apo form at pH 7.0, increased at pH 3.7 despite the decreased anisotropy. However, the hydrodynamic frictional ratio may be regarded as the product of a shape factor and a hydration factor (27). Structural frictional ratios derived from axial ratios, obtained from SAXS results by the use of Perrin's equation for a prolate ellipsoid of revolution (36) expressed in terms of frictional coefficients, decreased slightly between neutral and low pH whether derived from the $3V/(4\pi R_G^3)$ or the $R_G(S/V)$ relationship, as would be expected from the slightly lowered anisotropy. Assuming that the axial ratio fully reflects the frictional surface and that the frictional ratio derived from it truly represents the shape factor, one would conclude that the increase in the hydrodynamic frictional coefficient is due entirely to increased hydration of the protein.

Hydration values $h_1$ and $h_2$, determined by the hydrodynamic relationship (27) using the two structural frictional ratios derived from SAXS (i.e., $(f/f_0)_1$ from $(a/b)_1$, and $(f/f_0)_2$ from $(a/b)_2$) are presented in Table III. Also shown in this table is the degree of internal hydration $H$, derived from SAXS (Table I), as well as another SAXS parameter, the homogeneous hydration $H'$, derived according to Kratky (34) from the excess volume of $V$ over $\bar{v}$. For holoRBP, $H'$ and $H$ are in good agreement, whereas for apoRBP $H'$ is appreciably larger. Since $H'$ is based directly on the molecular volume, the larger change in $H'$ reflects the larger change in volume compared to that in $H$, referred to in the discussion of SAXS hydration above. The $h_1$ values, derived from the $3V/(4\pi R_G^3)$ relationship, at both pH values are much larger than any of the other corresponding quantities. This may apprear surprising, inasmuch as the usual method of determining an axial ratio is from the radius of gyration and volume relationship. However, since hydrodynamic friction is to a large extent a surface rather than merely a volume phenomenon, and since proteins

in general have irregular rather than smooth surfaces, it is $h_2$, rather than $h_1$, that should correspond to the SAXS parameters $H'$ and $H$ because $h_2$ is derived from the structural relationship sensitive to surface, $R_G$ $(S/V)$. The better agreement of $h_2$ at low pH with $H'$ than with $H$ is related to the fact that, like $H'$, $h_2$ is affected by the large volume change. Further, it might be expected that the opening of a cleft would increase the hydrodynamic frictional ratio to an extent not fully indicated by the axial ratio nor by the shape factor derived from it, with a resulting overestimation of the remaining hydrodynamic factor and therefore of $h_2$ as well as $h_1$. Compared to $h_1$, which is surface-independent, the surface-sensitive quality of $h_2$ can still provide most of the compensation for textural surface discussed above. Notwithstanding these differences, all parameters in Table III show increased protein hydration at the lower pH.

Comparison of the CD spectra for apoRBP at pH 7.0 and 3.7 (Fig. 5A) shows that the secondary structure of the protein is only slightly different. In the far uv region, the slight increase in negative ellipticity near 200 nm could be indicative of a more random structure, and such changes, though of greater magnitude, have been observed for the acid denaturation of immunoglobulin G (37). A more rigorous treatment of the CD data by the method of Chen *et al.* (29) failed to show significant changes in the calculated percentage of $\beta$-structure or $\alpha$-helix. On the other hand, the relatively large changes in the CD spectra observed in the near uv region (Fig. 5B) argue for a more disordered state for the residues asssociated with this region of the spectrum, that is, more freedom of rotation for the aromatic side chains (38). This would agree with the earlier mention of increased segmental motion and reversal of net charge and with the observation that the increase in molecular volume outpaced that in hydration. Increased exposure of aromatic groups in an opened aromatic-rich cleft would lead to less additional hydration than the increases in volume and surface would make one expect. The CD data obtained at pH 7.0 for holoRBP are in good agreement with the data given by Nishikimi and Kyogoka (7) and show a strong involvement of the aromatic residues of the protein in the binding of riboflavin. Disorientation of these residues (tyrosine and tryptophan) at low pH would lead to the release of riboflavin by the protein. The involvement of tyrosine and tryptophan in the binding of riboflavin by RBP has been demonstrated by chemical modification studies (8, 39). Thus the CD spectra show a marked change with respect to the chromophoric region of the protein, but this is accompanied by only small changes in the overall structure of the polypeptide backbone.

The observed changes in the molecular parameters of RBP can now be summed up to produce a coherent description of the changes in structure that accompany the release of riboflavin at low pH. RBP is shown by sedimentation equilibrium and electrophoresis to be a single-chain polypeptide exhibiting no dissociation or self-association at pH 7.0, in either presence or absence of riboflavin, and remaining monomeric at pH 3.7. SAXS results document a change in tertiary structure at low pH characterized by an appreciable increase in volume with slightly decreased anisotropy. Analysis of the total surface data gives an estimate of the portion attributable to increased surface texture of the molecule. The change in radius of gyration is of the order of magnitude associated with cleft closure in the case of several binding proteins reported in the literature (although the mechanism there was allosteric, whereas here it is pH induced). Sedimentation velocity data show unchanged tertiary sturcture on binding riboflavin at neutral pH and support the SAXS findings of increased hydration at low pH. Here the hydration values calculated from frictional coefficients by way of a surface-sensitive method agree with two sets of hydration values obtained by SAXS in two independent ways; those derived by a surface-independent method do not. Finally, the CD spectra indicate that the secondary structure of the protein does not change appreciably at low pH, whereas there is a dramatic change in aromatic residues known to be associated with ri-

boflavin binding. The mechanism emerging from these observations is based on solution properties alone since, in contrast to proteins for which similar mechanisms have been reported, no X-ray cystallographic data were available here. Subject to this reservation, the different lines of evidence are in substantial agreement and suggest that a picture consistent with all observations is one in which the release of riboflavin by RBP involves the opening of a preexisting aromatic-rich cleft in the protein molecule under conditions of low pH.

## REFERENCES


1. OSUGA, D. T., AND FEENEY, R. E. (1968) *Arch. Biochem. Biophys.* **124,** 560-574.
2. MAW, A. J. G. (1954) *Poultry Sci.* **33,** 216-271.
3. WINTER, W. P., BUSS, E. G., CLAGETT, C. O., AND BOUCHER, R. V. (1967) *Comp. Biochem. Physiol.* **22,** 897-906.
4. FARRELL, H. M., BUSS, E. G., AND CLAGETT, C. O. (1970) *Int. J. Biochem.* **1,** 168-172.
5. FROEHLICH, J. A., MERRILL, A. H., JR., CLAGETT, C. O., AND MCCORMICK, D. B. (1980) *Comp. Biochem. Physiol.* **66B,** 397-401.
6. BECVAR, J. E. (1973) Ph.D. Thesis, University of Michigan, Ann Arbor.
7. NISHIKIMI, M., AND KYOGOKA, Y. (1973) *J. Biochem. (Tokyo)* **73,** 1233-1242.
8. FARRELL, H. M., JR., MALETTE, M. F., BUSS, E. G., AND CLAGETT, C. O. (1969) *Biochim. Biophys. Acta* **194,** 433-442.
9. BLANKENKORN, G. (1980) *in* Flavins and Flavoproteins, Proceedings, Sixth International Symposium (Yagi, K., and Yamono, T., eds.), pp. 405-411, Japan Sci. Press, Tokyo.
10. LAEMMLI, U. K. (1970) *Nature (London)* **227,** 680-685.
11. LOWRY, O. H., ROSEBROUGH, N. J., FARR, A. L., AND RANDALL, R. J. (1951) *J. Biol. Chem.* **193,** 265-275.
12. SHIGA, K., HORIIKE, K., NISHINA, Y., OTANI, S., WATARI, H., AND YAMANO, T. (1979) *J. Biochem. (Tokyo)* **85,** 931-941.
13. HEMMERICH, P., VEEGER, C., AND WOODS, H. C. S. (1965) *Angew. Chem. Int. Ed.* **4,** 671-687.
14. KOZIOL, J. (1971) *in* Methods in Enzymology (McCormick, D. B., and Wright, L. D., eds.), Vol. 58, Part B, pp. 253-285, Academic Press, New York.
15. PESSEN, H., KUMOSINSKI, T. F., TIMASHEFF, S. N., CALHOUN, R. R., JR., AND CONNELLY, J. A. (1970) *Advan. X-Ray Anal.* **13,** 618-631.
16. PESSEN, H., KUMOSINSKI, T. F., AND TIMASHEFF, S. N. (1973) *in* Methods in Enzymology (Colowick, S. P., and Kaplan, N. O., eds.), Vol. 27, Part D, pp. 151-209, Academic Press, New York.
17. PESSEN, H., KUMOSINSKI, T. F., AND TIMASHEFF, S. N. (1971) *J. Agr. Food Chem.* **19,** 698-702.
18. LUZZATI, V., WITZ, J., AND NICOLAIEFF, A. (1961) *J. Mol. Biol.* **3,** 367-378.
19. LUZZATI, V., WITZ, J., AND NICOLAIEFF, A. (1961) *J. Mol. Biol.* **3,** 379-392.
20. LUZZATI, V. (1951) *Acta Crystallogr.* **10,** 136-138.
21. GUINIER, A. (1939) *Ann. Phys. (Paris)* **12,** 161-237.
22. PHILLIPS, J. W. (1963) Ph.D. Thesis, Pennsylvania State University, University Park.
23. POROD, G. (1951) *Kolloid Z.* **124,** 83-114.
24. SOULÉ, J. L. (1957) *J. Phys. Radium Phys. Appl. Suppl.* **18,** 90A-102A.
25. YPHANTIS, D. A. (1964) *Biochemistry* **3,** 297-317.
26. AUNE, K. C. (1978) *in* Methods in Enzymology (Hirs, C. H. W., and Timasheff, S. N., eds.), Vol. 28, Part F, pp. 163-185, Academic Press, New York.
27. SCHACHMAN, H. K. (1959) Ultracentrifugation in Biochemistry, pp. 129-131 and 215-247, Academic Press, New York.
28. SCHACHMAN, H. K., AND EDELSTEIN, S. J. (1973) *in* Methods in Enzymology (Colowick, S. P., and Kaplan, N. O., eds.), Vol. 27, Part D, pp. 3-59, Academic Press, New York.
29. CHEN, Y.-H., YANG, J. T., AND CHAU, K. H . (1974) *Biochemistry* **13,** 3350-3359.
30. MACDONALD, R. C., STEITZ, T. A., AND ENGELMAN, D. M. (1979) *Biochemistry* **18,** 338-342.
31. MACDONALD, R. C., ENGELMAN, D. M., AND STEITZ, T. A. (1979) *J. Biol. Chem.* **254,** 2942-2943.
32. PICKOVER, C. A., MCKAY, D. B., ENGELMAN, D. M., AND STEITZ, T. A. (1979) *J. Biol. Chem.* **254,** 11,323-11,329.
33. QUIOCHO, F. A., GILLILAND, G. L., NEWCOMER, M. E., MILLER, D. M., III, PFLUGRATH, J. W., SAPER, M. A., AND OLSON, J. S. (1980) *Fed. Proc.* **39,** 2103.
34. KRATKY, O. (1963) *in* Progress in Biophysics and Molecular Biology (Butler, J. A. V., Huxley, H. E., and Zirkle, R. E., eds.), Vol. 13, pp. 105-173, Pergamon, New York.
35. SVEDBERG, T., AND PEDERSEN, K. O. (1940) The Ultracentrifuge, pp. 1-41, Clarendon Press, Oxford.
36. PERRIN, F. (1936) *J. Phys. Radium* **7,** 1-11.
37. DOI, E., AND JIRGENSONS, B. (1970) *Biochemistry* **9,** 1066-1073.
38. BEYCHOK, S. (1966) *Science* **154,** 1288-1299.
39. BLANKENHORN, G. (1978) *Eur. J. Biochem.* **82,** 155-160.
40. ONCLEY, J. L. (1941) *Ann. N.Y. Acad. Sci.* **41,** 121-150.